Dalton Transactions

ROYAL SOCIETY OF CHEMISTRY

PAPER

View Article Online
View Journal | View Issue

Cite this: *Dalton Trans.*, 2024, **53**, 17880

Three organic–inorganic polyoxoniobate-based compounds modified with Cu(II) amine complexes: synthesis, characterization, and catalytic studies for oxidation of styrene†

Zhi-Cheng Duan, Guanghua Li, Ke-Chang Li and Xiao-Bing Cui *

Received 6th September 2024,
Accepted 12th October 2024

DOI: 10.1039/d4dt02544j

rsc.li/dalton

Three novel organic–inorganic polyoxoniobate-based compounds modified with Cu(II) amine complexes were synthesized under hydrothermal conditions with the chemical formulas as follows: $K_{0.5}[Cu(enMe)_2]_4[K_{0.5}SiNb_{12}O_{40}(VO)_{4.25}](OH)_{1.5}\cdot 9H_2O$ (**1**), $K_{0.5}[Cu(enMe)_2]_4[K_{0.5}H_2PNb_{12}O_{40}(VO)_2]\cdot 12.5H_2O$ (**2**), and $K_{0.5}[Cu(enMe)_2]_4[K_{0.5}H_2VNb_{12}O_{40}(VO)_2]\cdot 12.5H_2O$ (**3**) (enMe = 1,2-diaminopropane). These compounds were characterized by single crystal X-ray diffraction, infrared spectroscopy (IR), UV-Vis spectroscopy, elemental analysis and powder X-ray diffraction (PXRD) analysis. Notably, while these three compounds exhibit identical cell parameters, they possess distinct stoichiometric compositions and differing polyoxometalate building block structures. Typically, compounds with the same cell parameters are classified as isostructural, sharing identical structures with only minor elemental variations in their compositions. To the best of our knowledge, compounds **1–3** represent the first instances of compounds that share the same cell parameters yet are not isostructural. In this study, we not only synthesized these three compounds and thoroughly examined the differences in their structures and properties, but also investigated their catalytic performances as catalysts for the oxidation of styrene.

Introduction

Metal–oxygen cluster compounds are a class of compounds consisting of early transition metal ions such as vanadium, niobium, molybdenum, and tungsten covalently linked with oxygen atoms to form multi-nucleated or highly nucleated compounds.[1–3] Because of their chemical properties such as high surface negative charge density and favorable redox properties, they have important applications in the fields of catalysis, magnetism, and energy conversion,[4–6] and are currently a hot spot in multidisciplinary research. However, the rapid development of polyoxoniobates (PONb) has occurred only in recent decades compared to other POMs containing Mo, W or V, due to the fact that the inert Nb precursors can only exist in strongly alkaline aqueous solutions, which are difficult to be obtained by conventionalization under acidification conditions.[7–9]

In recent years, the chemistry of niobium polyoxoanions has undergone rapid development, and their cluster structure system has become increasingly larger.[8] Initially, the synthesis of niobopolyacids was mostly centered around iso-polyoxoniobates (IPONbs), and some building blocks such as $\{Nb_7O_{22}\}$,[10] $\{Nb_{24}O_{72}\}$,[11] $\{Nb_{32}O_{96}\}$,[12] $\{Nb_{10}O_{28}\}$,[13] $\{Nb_{27}O_{76}\}$,[14] $\{Nb_{47}O_{134}\}$,[15] *etc.*, were constructed. Subsequently, the synthesis of heteropolyniobates (HPONbs) was achieved by modifying niobopolyacids at the atomic level through the introduction of heteroatoms (such as Si, P, V, *etc.*),[16,17] and most of them were focused on the Nb-Keggin-type and capped Nb-Keggin-type derivatives. In 2002, Nyman's group reported the first heteropolyoxoniobate $K_{12}[Ti_2O_2][SiNb_{12}O_{40}]\cdot 16H_2O$.[18] Following this, the same group has also reported additional similar Keggin-type HPONBs $\{TNb_{12}O_{40}\}[T = Si, Ge]$.[19] In subsequent studies, heteroatoms were also referenced to As, Te, and S atoms, resulting in the synthesis of $\{AsNb_{12}\}$,[20] $\{Te_2Nb_{24}\}$,[21] and $[SNb_8]$.[22] In the reported capped Nb-Keggin structures, Nb, Sb, Ti, and V atoms are generally introduced as capping atoms. Feng, Hill and others have further reported a variety of capped polyoxoniobates, such as $[Nb_2O_2(H_2O)_2][SiNb_{12}O_{40}]^{10-}$,[17] $[Ti_2O_2][GeNb_{12}O_{40}]^{12-}$,[23] $\{[Sb_2O_2][XNb_{12}O_{40}]\}^{n-}$ (X = Si, Ge, V, P, As),[24] $\{VNb_{12}O_{40}(VO)_2\}$,[25] $\{PNb_{12}O_{40}(VO)_6\}$[26] and so on.

College of Chemistry and State Key Laboratory of Inorganic Synthesis and Preparative Chemistry, Jilin University, Changchun, Jilin, 130023, P. R. China. E-mail: cuixb@mail.jlu.edu.cn

†Electronic supplementary information (ESI) available. CCDC 2378667 for compound **1**, 2378668 for compound **2**, and 2378669 for compound **3**. For ESI and crystallographic data in CIF or other electronic format see DOI: https://doi.org/10.1039/d4dt02544j

In the context of niobium polyoxometalate synthesis, a number of polyoxoniobates with the same cell parameters and isostructural characteristics have been documented. Notably, In 2012, Nyman's group first introduced third main group elements into heteropolyniobates, and obtained two isostructural examples of poly-niobate anions, specifically $[Al/GaNb_{18}O_{54}]^{15-}$.[27] Subsequently, in 2015, Peng's group reported the synthesis of $\{[Sb_2O_2][XNb_{12}O_{40}]\}^{n-}$ (X = Si, Ge, V, P, As),[24] which included five isostructural examples of crystals sharing the same cell parameters. However, in the present work, we synthesized three crystals that possess identical cell parameters as examples, and among these, compounds **2** and **3** are confirmed to be isostructural to each other; however, compound **1** shows an unprecedented feature. Although compound **1** shows the same cell parameters as compounds **2** and **3**, it is not thoroughly isostructural to those two compounds, but presents significant structural differences between the structures of compounds **2** and **3**. To the best of our knowledge, such a difference between similar structures has not been previously reported. The compounds under investigation include $K_{0.5}[Cu(enMe)_2]_4[K_{0.5}SiNb_{12}O_{40}(VO)_{4.25}](OH)_{1.5}9H_2O$ (**1**), $K_{0.5}[Cu(enMe)_2]_4[K_{0.5}H_2PNb_{12}O_{40}(VO)_2]\cdot12.5H_2O$ (**2**), and $K_{0.5}[Cu(enMe)_2]_4[K_{0.5}H_2VNb_{12}O_{40}(VO)_2]\cdot12.5H_2O$ (**3**) (enMe = 1,2-diaminopropane). The Keggin anion clusters in compounds **1**, **2**, and **3** are centered on Si, P and V, respectively. The Keggin clusters feature six square windows within the $\{XNb_{12}O_{40}\}$ (X = Si, P and V) Keggin framework; for $\{SiNb_{12}O_{40}(VO)_{4.25}\}$ in compound **1**, five of the six square windows were capped by four 100% occupied {VO} groups and one 25% occupied {VO} group. With respect to compounds **2** and **3**, there are only four half-occupied vanadium atoms capping the four equatorial windows within the Keggin core. Furthermore, we employed compounds **1–3** as catalysts for the catalytic oxidation reaction of olefins and evaluated the catalytic performances of these three compounds for styrene oxidation to styrene oxide. In addition, we also carefully discussed the influence of the subtle difference of the structures on the catalytic efficiencies.

Experimental

Materials and methods

All chemicals were of analytical reagent grade quality, commercially purchased and used without further purification. The precursor $K_7HNb_6O_{19}\cdot13H_2O$ was synthesized and characterized by IR spectroscopy according to the literature.[28] Fourier transform infrared (FT-IR) spectra were recorded using a PerkinElmer Spectrum One FT-IR spectrophotometer and the samples were prepared as KBr pellets. UV-vis spectra were obtained using a Shimadzu UV-3100 spectrophotometer. X-ray diffraction (XRD) measurements were performed by using a Cu Kα source on a powder diffractometer (Scintag X1). Elemental analyses for C, H, and N were performed on a PerkinElmer 2400 CHN elemental analyser. The chemical compositions of the samples were determined by inductively coupled plasma-optical emission spectroscopy (PerkinElmer Optima 3300DV).

Synthetic procedures

General procedure for the synthesis of compound 1. Compound **1** was synthesized by a hydrothermal method. For solution A, $VOSO_4$ (0.0326 g, 0.2 mmol) was dissolved in 4 mL distilled water, then one drop of hydrazine hydrate was added and the solution was stirred for half an hour. Then $K_7HNb_6O_{19}\cdot13H_2O$ (0.15 g, 0.11 mmol) and $Na_2SiO_3\cdot9H_2O$ (0.32 g, 0.11 mmol) were added to solution A. For solution B, $CuCl_2\cdot2H_2O$ (0.1 g, 0.58 mmol) and enMe (2.32, 2 mL) were dissolved in deionized water (3 mL) in sequence. After stirring for 0.3 h, solution A was added drop-wise into B, and then, Na_2SO_4 (0.0142 g, 0.1 mmol) was added to the mixture and stirring was continued for another 1 h. Finally, the solution was sealed in a 25 ml Teflon-lined autoclave and heated under autogenous pressure at 160 °C for 3 days. After cooling down to room temperature, brownish-purple needle-like crystals suitable for single-crystal X-ray diffraction were obtained. Elemental analysis: found: C: 9.11%, H, 2.92%, N: 7.12%, Si: 1.06%, Cu, 7.88%, V: 6.52%, Nb: 35.21%. Calculated: C: 9.18%, H: 3.19%, N: 7.14%, Si: 0.89%, Cu: 8.09%, V: 6.89%, Nb: 35.49%.

General procedure for the synthesis of compound 2. The synthesis procedure of compound **2** is the same as that for compound **1**, but $Na_2SiO_3\cdot9H_2O$ is replaced by $NaH_2PO_4\cdot12H_2O$ (0.0716 g, 0.2 mmol) and the amount of $CuCl_2\cdot2H_2O$ was changed to 1 mmol. Finally, the solution was sealed in a 25 ml Teflon-lined autoclave and heated under autogenous pressure at 160 °C for 3 days. After cooling down to room temperature, brownish-purple needle-like crystals suitable for single-crystal X-ray diffraction were obtained. Elemental analysis: found: C: 9.37%, H: 3.25%, N: 7.33%, P: 0.94%, Cu: 8.12%, V: 3.30%, Nb: 36.36%. Calculated: C: 9.50%, H: 3.56%, N: 7.39%, P: 1.02%, Cu: 8.38%, V: 3.36%, Nb: 36.76%.

General procedure for the synthesis of compound 3. Compound **3** was synthesized as follows: $K_7HNb_6O_{19}\cdot13H_2O$ (0.15 g, 0.11 mmol) was dissolved in 7 mL of H_2O to obtain a colorless solution, and then $VOSO_4$ (0.1 g, 0.3 mmol), $CuCl_2\cdot2H_2O$ (0.17 g, 1 mmol), and enMe (2.32, 2 mL) were added sequentially and stirred for 30 min, followed by the addition of 0.1 g Tris (Trometamol). Then the solution was stirred again for 20 min, and the mixture was sealed in a 25 mL Teflon-lined stainless-steel reactor and heated at 160 °C. After cooling down to room temperature, brownish-purple needle-like crystals suitable for single-crystal X-ray diffraction were obtained. Found: C: 9.31%, H: 3.37%, N: 7.26%, Cu: 8.12%, V: 5.11%, Nb: 36.29%. Calculated: C: 9.44%, H: 3.53%, N: 7.34%, Cu: 8.33%, V: 5.01%, Nb: 36.52%.

Crystallography

The single-crystal diffraction data of compounds **1–3** were obtained on a Bruker Smart-CCD diffractometer with Mo K_α radiation (λ = 0.710 73 Å). The data were collected at tempera-

tures 300(2), 211(2), and 200(2) K for compounds **1–3**, respectively. The solutions of compound **1–3** structures were obtained using SHELXL-2014/7[29,30] and Olex 2[31] programs and the position of heavy atoms was determined by the direct method. The coordinates of all non-hydrogen atoms were derived and corrected in the refinement process using the least squares method, hydrogenation was performed using theoretical hydrogenation, and anisotropy was implemented for all non-hydrogen atoms. Some undissolved A-Alerts have been explained as validation reply forms in the CIF files. Crystal data are listed in Table S1.† CCDC numbers: 2378667 for compound **1**, 2378668 for compound **2**, and 2378669 for compound **3**.†

Results and discussion

Crystal structure of compound 1

Single-crystal X-ray diffraction analysis shows that compound **1** crystallizes in a tetragonal space group of *I*4/*mcm*. Compound **1** exhibits a two-dimensional organic–inorganic skeleton connected by $[SiNb_{12}O_{40}(VO)_{4.25}]^{7.5-}$ and $[Cu(enMe)_2]^{2+}$ (Fig. 1d). The K atoms form a K–N bond by coordinating with the nitrogen atoms of the enMe organic ligand, which has been very rare in previous syntheses (Fig. 1c).[32] The cluster $[SiNb_{12}O_{40}(VO)_{4.25}]^{7.5-}$ has a classical Keggin type anion $[SiNb_{12}O_{40}]^{16-}$ with 4 and 0.25 {VO} capping units (Fig. 1a). There are six square windows within the $[SiNb_{12}O_{40}]^{16-}$ anion, five of which were capped by four {VO} groups and by a 0.25-occupied {VO} group, while the sixth window was capped by a K ion with K–O distances in the range of 2.6–3.2 Å. It should be noted that the bi-capped Keggin units have been widely investigated, with bi-capped polyoxoniobates being the mostly studied ones in polyoxoniobate chemistry. However, the tetra-capped variants have rarely been reported.[17,23,25] In terms of the hexa-capped ones, polyoxoniobates with this type of Keggin structure have been reported and carefully investigated by Wang *et al.*[26] The six capping atoms of Wang's compounds are identical, all being vanadium. Conversely, in our compound, four of the capping atoms are vanadium atoms, one is 0.25 vanadium and the final one is 0.5 potassium. Consequently, the four windows at the equatorial positions of $[SiNb_{12}O_{40}]^{16-}$ can be viewed as being capped by four $\{VO_5\}$ square pyramids, while one of the two polar position windows is covered by a 0.25 occupied vanadium and the other one of the polar position windows is covered by a 0.5 potassium atom. The symmetry of the Keggin core of the polyoxoniobate is destroyed by capping vanadiums and particularly by the capping potassium, as shown in Fig. 1a and b; the capped polyoxoniobate looks like a pineapple with the capping potassium.

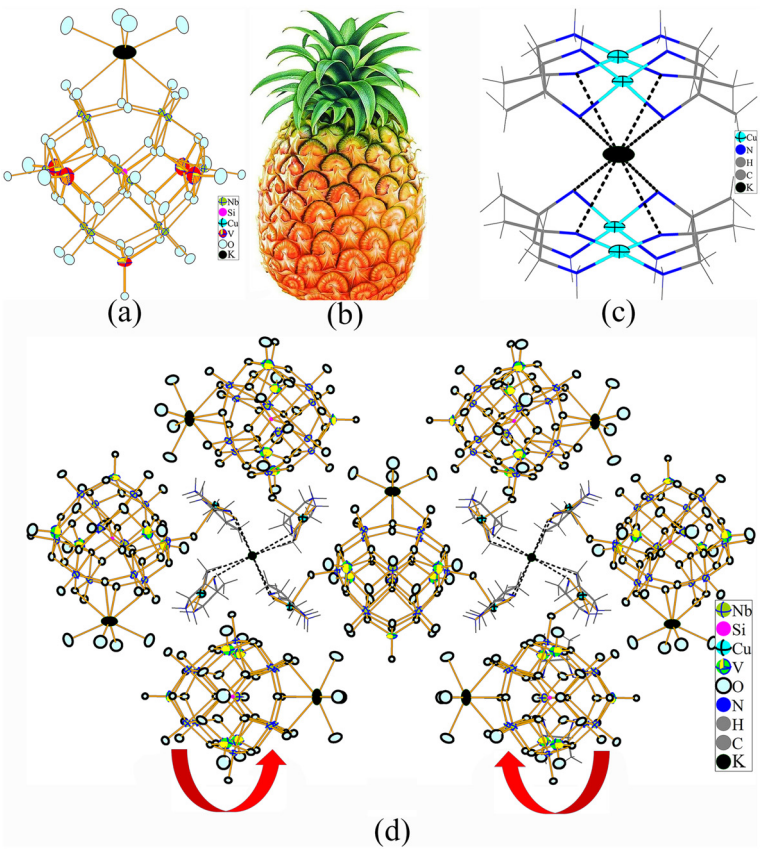

Fig. 1 (a and b) Ellipsoid representation of the pineapple like cluster in compound **1**; (c) ellipsoid and wire representation of the windmill shaped unit in compound **1**; and (d) the two-dimensional framework in compound **1**.

The $[SiNb_{12}O_{40}(VO)_{4.25}]^{7.5-}$ clusters have three types of oxygens, including 16 and 1/4 terminal oxygens (O_t), 24 bridging oxygens (O_b) and four central oxygens (O_c). The lengths of the V–O_t, and V–O_b bonds are 1.57(4)–2.312(16) Å and 1.603(11)–2.127(9) Å, respectively. The lengths of the Nb–O_t, Nb–O_c, and Nb–O_b bonds are 1.753(10)–2.004(7) Å, 1.755(7)–2.450(6) Å, and 1.777(13)–2.413(11) Å, respectively.

In the two-dimensional framework, each $[SiNb_{12}O_{40}(VO)_{4.25}]^{7.5-}$ is connected to four $[Cu(enMe)_2]^{2+}$ segments *via* the interactions between the copper centre of the complex and the terminal oxygens of the {NbO_6} octahedron of the cluster. Subsequently, four neighbouring $[Cu(enMe)_2]^{2+}$ complexes are then connected to a potassium atom *via* eight K–N bonds with a length of 3.387 Å, resulting in the formation of a windmill shaped unit, where the $[Cu(enMe)_2]^{2+}$ complexes function as blades. Each Cu^{II} cation adopts a tetra-coordination, defined by four N atoms from two enMe organic ligands and a terminal oxygen from $[SiNb_{12}O_{40}(VO)_{4.25}]^{7.5-}$. One pineapple cluster is linked to two windmill units, while a single windmill unit joins four pineapple clusters, therefore, establishing a two-dimensional framework structure (Fig. 1d). It should be noted that the orientations of the four pineapple clusters around the windmill exhibit intriguing characteristics; the four orientations of the four pineapple clusters around one windmill points to the clockwise direction, whereas the four orientations of the four pineapple clusters around the adjacent windmill point to the counterclockwise direction.

Crystal structures of compounds 2 and 3

Single-crystal X-ray diffraction analysis shows that compounds **2** and **3** both crystallize in a tetragonal space group of *I*4/*mcm* with almost identical cell parameters as compound **1**, but anionic clusters $[PNb_{12}O_{40}(VO)_2]^{11-}$ and $[VNb_{12}O_{40}(VO)_2]^{11-}$ in compounds **2** and **3** have a significant difference from $[SiNb_{12}O_{40}(VO)_{4.25}]^{7.5-}$ found in compound **1**.

Despite differing in their central heteroatoms, compounds **2** and **3** have the same cluster structures and are isostructural to each other but both are not isostructural to compound **1**. Here we chose compound **2** as the representative to specify their structure. The $[PNb_{12}O_{40}(VO)_2]$ cluster in compound **2** can be described as a modified Keggin unit, wherein one phosphorus atom is the heteroatom centre and four half vanadium atoms cover its four equatorial pits. The Keggin core is consistent with that in compound **1** with the same six square windows; however, there are only four half-vanadium atoms capping the four equatorial windows of the Keggin core, which markedly contrasts with the capped cluster observed in compound **1**. The primary capped Keggin structure of compound **1** is thoroughly distinct from those of compounds **2** and **3**. Nevertheless, the secondary extended structure of compound **1** closely resembles those of compounds **2** and **3**, resulting in the three compounds exhibiting nearly identical cell parameters.

The synthesized compounds **1**, **2** and **3** provide compelling examples of compounds with nearly identical secondary structures but different stoichiometric compositions. Consequently, compounds **2** and **3** are isostructural to each other, but the two are not isostructural to compound **1**.

There are four and a 0.25 vanadium covering the five pits of the six ones of the Keggin core in compound **1**. In contrast, there are only four 0.5 vanadiums capping the four pits of the six ones of the Keggin core in compounds **2** and **3**. A notable distinction between the cluster structures of compound **1** and compounds **2** and **3** is that the apical position of the Keggin core in compound **1** is capped by a 0.25 vanadium, whereas the corresponding apical cluster windows of the Keggin core in compounds **2** and **3** remain uncapped. Additionally, the four sites of the equatorial Keggin windows in compound **1** are occupied by four vanadium atoms with an occupancy factor of **1**, while the four corresponding sites are occupied by four half-occupied vanadiums in compounds **2** and **3**. BVS calculations reveal (Table S2†) that the oxidation states of all the niobium atoms in the three compounds are +5. In contrast, all capped vanadium atoms exhibit a +4 oxidation state, while the central vanadium atom in compound **3** is characterized by a +5 oxidation state.[33]

The diameter of the capped Keggin core, measured from one terminal oxygen from a capped vanadium to the most distant terminal oxygen from a centre-symmetrically related capped vanadium, is approximately 11.35 Å. In comparison, the distance between the two most distant terminal oxygens from two equatorial niobium atoms within the Keggin core is 10.89 Å, meaning that the capping of the vanadiums on the windows of the Keggin core does not significantly alter the overall shape of the Keggin cluster. Therefore, while the primary structures of compound **1** and compounds **2** and **3** are stoichiometrically different, their secondary structures based on these different primary structures are almost identical; hence the three have almost the same cell parameters but are not isostructural.

Recently, a compound closely resembling compound **1** was reported by Dang's group.[32] The primary cluster structure of the Dang's compound exhibits significant similarities to that of compound **1**, characterized by the presence of 4.25 vanadium atoms capping the Keggin core. However, it is noteworthy that the sixth cluster window in Dang's compound is not capped by a potassium atom in contrast to compound **1**. The bicapped polyoxoniobate was first synthesized (Fig. 2b and c),[17,22–25] some years later, tetracapped polyoxoniobate was synthesized (Fig. 2d),[20,32] and the hexacapped ones (Fig. 2e) also were synthesized.[26] Although the primary building cluster structures of these compounds seem to have close relationship with each other, the secondary structures of these compounds are markedly different, complicating the determination of whether these clusters are intermediates between the Keggin and hexacapped Keggin ones. The synthesis of compounds **1–3** gives solid evidence that both the bicapped and tetracapped (or pentacapped) variants function as intermediates between the Keggin and hexacapped Keggin clusters, as their secondary structures are almost identical despite differences in their primary cluster structures. This means that the cluster differences of these series intermediates will not sig-

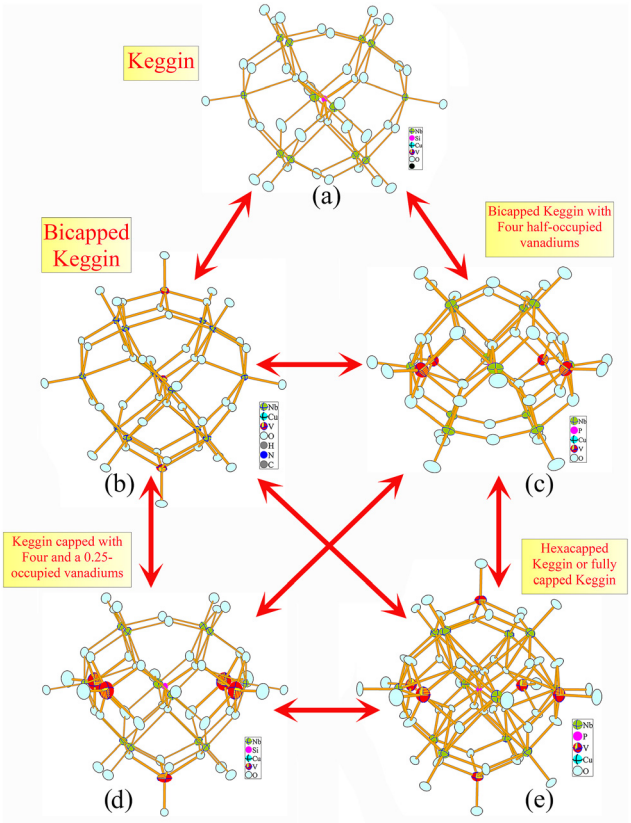

Fig. 2 (a) Ellipsoid representation of the Keggin cluster; (b) the bicapped Keggin cluster reported by Hu's group;[25] (c) the bicapped Keggin cluster in compound **2**; (d) the Keggin cluster capped by 4.25 vanadiums in compound **1**; and (e) the hexacapped Keggin cluster reported by Wang' group.[26]

nificantly influence their stacking extended structures. Thus, compounds **2** and **3**, along with the Dang's compound[32] and compound **1** can be viewed as four intermediates situated between the Keggin core and the hexacapped Keggin core reported by Wang *et al.* (Fig. 2).[26]

Characterization

IR, UV-Vis and PXRD analyses. The IR spectra of compounds **1–3** are shown herein. Since compounds **1–3** have similar metal–organic complexes and polyoxometalates, each of which consists of $[Cu(enMe)_2]^{2+}$ as a metal complex and similar polyoxoniobates, specifically $\{SiNb_{12}O_{40}(VO)_{4.25}\}$ or $\{XNb_{12}O_{40}(VO)_2\}$ (X = P, V), their FT-IR properties exhibit significant similarities. The FT-IR spectrum of compound **1** is illustrated in Fig. 3; the absorption band at 1590–1060 cm^{-1} corresponds to the vibrational frequencies of the enMe ligand in compound **1**. For compounds **2** and **3**, the characteristic peaks of organic ligands are identified at 1590–1060 and 1590–1060 cm^{-1}, respectively. The IR spectrum of compound **1** is shown in Fig. 3a. The weak peak at 972 cm^{-1} is associated with the terminal V=O stretch $\nu(V{=}O_t)$. The bands characteristic of $\nu(V{=}O_t)$ indicate the existence of V^{4+} sites: clusters that are formed by exclusively V^{4+} generally exhibit $\nu(V{=}O_t)$ bands

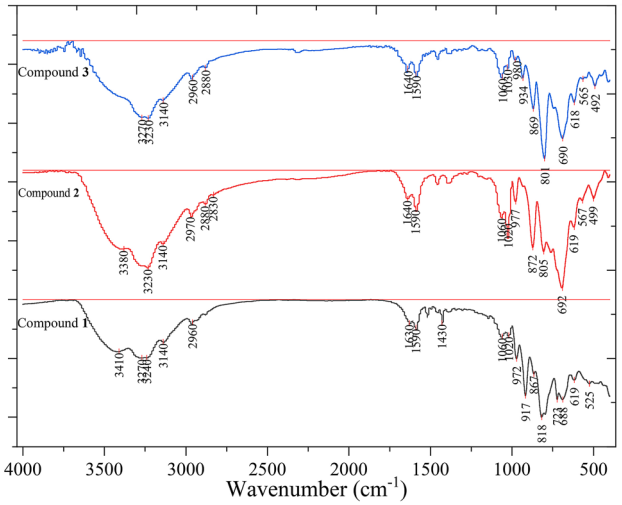

Fig. 3 The FT-IR spectra of compounds **1–3**.

in the range of 970–1000 cm^{-1}, while the bands in the region 940–960 cm^{-1} come from the presence of V^{5+}. The detection of absorbance in the 970–1000 cm^{-1} region provides a valuable diagnostic for the presence of V^{4+} centres.[34] The strong bands at 867 and 818 cm^{-1} are attributed to $\nu(Nb–O_t)$, while the strong bands at 688 and 525 cm^{-1} are ascribed to $\nu(Nb–O_b–Nb)$. The IR characteristic peaks of compound **2** are depicted in Fig. 3, with the peak position of 977 cm^{-1} ascribed to the presence of V^{4+} in the cluster of compound **2**.[34] 872 and 805 cm^{-1} as well as 692 and 499 cm^{-1} absorption peaks are attributed to $\nu(Nb–O_t)$ and $\nu(Nb–O_b–Nb)$ stretching vibration and bending vibration frequencies, respectively. The IR characteristic peaks of compound **3** are shown in Fig. 3 with peaks at 980 due to the existence of V^{4+} centers,[34] and 869 and 801 cm^{-1} as well as 690 and 492 cm^{-1} absorption peaks attributed to $\nu(Nb–O_t)$, and $\nu(Nb–O_b–Nb)$ stretching vibration and bending vibration frequencies, respectively. The spectral features observed across the three compounds demonstrated that the three compounds contains similar vanadium capped polyoxoniobates and analogous copper coordination complexes with identical organic ligands.

FT-IR spectroscopy is a very powerful analytical technique, and can also be used to discern the subtle structural differences between the three compounds. In the IR spectrum of compound **1**, a strong characteristic band at 917 cm^{-1} is attributed to $\nu(Si–O_c)$ frequency, and it should be noted that this particular band only can be observed in the spectrum of compound **1**, as the heteroatom of the Keggin core of compound **1** is Si.[35] In contrast, the IR spectrum compound **2** reveals a strong band at 1020 cm^{-1}, which can be attributed to the superposition of two overlapping components: one associated with $\nu(P–O_c)$ and the other linked to the enMe organic ligands like those in compounds **1** and **3**. Therefore, the peak intensity of this band in compound **2** is significantly greater than those observed in compounds **1** and **3**. The relative peak intensity ratio of the band at around 1020 cm^{-1} and the highest peak in

the IR spectrum of compound **2** is approximately 1 : 1.7, whereas the corresponding intensity ratios for compounds **1** and **3** are 1 : 3.2 and 1 : 4, respectively, indicating that the band around 1020 cm^{-1} in compound **2** originates from both the vibrations of P–O bonds and enMe organic ligands.

The IR spectrum of compound **3** displays a peak at 934 cm^{-1}, which is attributed to the presence of vanadium in the +5-oxidation state (V^{5+}), a feature not observed in the spectra of both compounds **1** and **2**. This absence can be explained by the fact that only compound **3** incorporates vanadium(v) as the heteroatom in its Keggin core.

The X-ray powder diffractograms of compounds **1–3** agree well with the simulated XRD patterns, thereby confirming the phase purity of all the compounds (Fig. S1†). Variations in reflection intensity may be due to the preferred orientation in the powder samples of these compounds.

The UV-vis spectra of compounds **1–3** are shown in Fig. S2 (a–c)† in the wavelength range of 200–500 nm. The UV-vis spectra of compounds **1–3** are more similar. The spectra of these compounds exhibit notable similarities. Specifically, the UV-vis spectra of compounds **1–3** demonstrate a pronounced absorption peak accompanied by a distinct shoulder at approximately 203 nm and 247 nm for compound **1**, 204 nm and 245 nm for compound **2**, and 204 nm and 250 nm for compound **3**. These features are likely attributed to the charge transfer absorption peaks associated with O → Nb in the three compounds.

Epoxidation of styrene

Metal-oxo clusters are recognized as excellent catalysts widely used in industry due to their remarkable photothermal stability and good redox properties.[36–38] In contrast, the catalytic oxidation of PONbs has received comparatively less attention than other polymetallic oxides containing Mo, W or V. The development of niobium-based polymetallic oxides that demonstrate superior catalytic activity in organic reactions remains a significant chemical challenge.

The oxidation of styrene has long been an important process since styrene oxide has been an important synthetic intermediate in the synthesis of fragrances, epoxy resins, plasticizers, pharmaceuticals, sweeteners and fine chemicals.[39] Numerous different research groups from all over the world have devoted themselves to the development of the oxidation of styrene using various different traditional POMs, POM derivatives and composites formed by heterogenizing homogeneous POMs onto diverse solid supports.[40–56] Unfortunately, it is noteworthy that the majority of previously reported POM catalysts or POM-based composite catalysts preferentially convert styrene to benzaldehyde rather than styrene oxide.[40–56] This preference can be attributed to the mechanism pathway of styrene oxidation, which involves the formation of a styrene oxide as an intermediate, and acidic conditions tend to promote the hydrolysis of styrene oxide, leading to the production of benzaldehyde.[57] Given that most traditional POMs are synthesized under acidic conditions or almost all the traditional POMs show strongly acidic properties,[58] their use as catalysts for styrene oxidation will inevitably result in the formation of benzaldehyde.[40–56]

Only a few research studies utilizing such POM catalysts have successfully yielded styrene oxide as the main product; however, these studies typically employed short reaction times, resulting in lower conversions in exchange for higher selectivity towards styrene oxide.[59] Consequently, catalytic systems based on traditional POMs are unsuitable for the production of acid sensitive epoxides because epoxide ring-opening occurs under acidic conditions.[60] So, finding a suitable POM catalytic system for the production of epoxides is considerably challenging.

However, the PONb POMs, synthesized under strongly alkaline conditions, show much stronger basic properties compared to traditional acidic POMs.[7–9] Therefore, the unique basic characteristics of PONbs enable them to inhibit acid-catalyzed epoxide hydrolysis, leading to the production of styrene oxides.[57]

Based on the aforementioned points, we employed PONbs as catalysts for the catalytic epoxidation of styrene, which provides an environmentally sustainable route for the production of styrene oxide. In this paper, we performed experiments to test the catalytic ability of *tert*-butyl hydroperoxide (TBHP) aqueous solution as an oxidizing agent and compounds **1–3** as catalysts to oxidize styrene in an intermittent reactor. In a typical run, the catalyst (2 mg), *tert*-butyl hydroperoxide (274 μL, 2 mmol), styrene as the substrate (114 μL, 1 mmol), and acetonitrile as solvent (2 mL) were transferred to a (5 mL) double-necked round-bottom flask. The mixture was stirred in an oil bath and heated to 40 °C, 60 °C or 80 °C. The content of the mixture was quantified using a gas chromatograph (Shimadzu, GC-8A) equipped with an FID detector and a capillary column (SE-54, 30 m × 0.53 mm × 1.0 μm) and identified by comparison with authentic samples and GC-MS coupling. In addition, the conversion and selectivity of reactions were analysed by gas chromatography and the area normalization method.

In the olefin oxidation reactions we used compound **1** as a catalyst in order to achieve the optimum reaction conditions, and the effects of various factors, including catalyst dosage, solvent type, reaction temperature and other factors, on the catalysis results were systematically explored. Initially, the optimum dosage of the catalyst optimized for this reaction was evaluated (Table 1, entries 2–4). It was observed that increasing the dosage of compound **1** from 1 mg to 2 mg resulted in an enhancement of the conversion rate from 88.4% to 95.2% and an increase in selectivity towards styrene oxide from 14.1% to 57.6%. However, upon further increasing the catalyst dosage to 3 mg, the conversion rate exhibited only a marginal increase to 95.9%, while the selectivity for styrene oxide declined to 37.3%. This indicated that a catalyst dosage of 2.0 mg was a better choice, so we chose 2.0 mg for subsequent experiments. Following this, the type of solvent used for this reaction was optimized. Here, acetonitrile, methanol, ethanol, and *n*-hexane were selected for their effectiveness (Table 1, entries 3 and 5–7). By screening the solvents, it is clearly observed that aceto-

Table 1 Selectivities and conversions of different catalysts with different dosages and solvents

Entry	Catalyst	Solvent	Dosage	Conv. (%)	Sel. (%)		
					So	Bza	Other
1	Blank	CH_3CN	0 mg	33.4	29.0	59.5	11.5
2	Compound **1**	CH_3CN	1 mg	88.4	14.1	77.7	8.2
3	Compound **1**	CH_3CN	2 mg	95.2	57.6	36.0	6.4
4	Compound **1**	CH_3CN	3 mg	95.9	37.3	39.5	23.2
5	Compound **1**	MeOH	2 mg	28.8	95.7	4.2	0.1
6	Compound **1**	EtOH	2 mg	27.8	16.7	74.0	9.3
7	Compound **1**	*n*-Hexane	2 mg	62.9	86.2	4.6	9.2

Reaction conditions: TBHP (2 mM, 274 μL), styrene (1 mM, 114 μL), solvent (2 mL), 80 °C, and 8 h reaction time. Bza, benzaldehyde; So, styrene oxide; and others, including benzoic acid and phenylacetaldehyde.

nitrile as a solvent shows good performance in terms of conversion and selectivity. Therefore, acetonitrile was selected as the solvent for further experiments.

In order to investigate the influence of temperature on the reaction, catalytic experiments were conducted at 40, 60 and 80 °C, respectively. As shown in Table 2, for compound **1**, both the conversion and selectivity of styrene oxide exhibited a notable increase, rising from 73% (40 °C) to 95.2% (80 °C) and 31.9% (40 °C) to 57.6% (80 °C), respectively. Therefore, 80 °C was selected as the optimum reaction temperature.

The kinetic behaviour of the reaction was analysed from the catalysis data obtained during the 1st hour of the reaction at different temperatures of 40, 60 and 80 °C. As can be seen from Fig. 4, compound **1** shows a linear relationship between $\ln(C_t/C_0)$ and reaction time at 80 °C, 60 °C and 40 °C. Analysis of the results from the figures shows that the catalytic reaction data are consistent with the kinetic characteristics of the first order reaction.

$$\frac{dC_t}{dt} = kC_t \quad (1)$$

$$\ln\frac{C_0}{C_t} = kt \quad (2)$$

$$\ln k = -\frac{E_a}{RT} + \ln A \quad (3)$$

The kinetic behaviour of compound **1** as a catalyst can be studied using the Arrhenius equation. In this context, eqn (1)–(3) define C_t, C_0, k, and t as the concentration at time t, the initial concentration at the beginning of the reaction, the reaction rate constant, and the reaction time, respectively. According to eqn (1) and (2), the slope of the resulting graph represents the reaction rate constant, allowing for the calculation of the value of k. The observed slopes for compound **1** were 0.0013 min^{-1} at 40 °C, 0.00396 min^{-1} at 60 °C and 0.00886 min^{-1} at 80 °C (Fig. 4a, b and c). Furthermore, the apparent activation energy E_a of the oxidative reaction was calculated to be 44.6 kJ mol^{-1} according to eqn (3) (Fig. 4d).

Table 2 Catalytic effects of compound **1** at different temperatures

Entry	Temp (°C)	Conv. (%)	Sel. (%)			K (min^{-1})
			So	Bza	Other	
1	40	73.0	31.9	66.7	1.4	0.00130
2	60	92.9	13.0	84.7	2.3	0.00396
3	80	95.2	57.6	36.0	6.4	0.00886

Reaction conditions: catalyst (2 mg), TBHP (2 mM, 274 μL), styrene (1 mM, 114 μL), CH_3CN (2 mL), and 8 h reaction time.

Based on the above experimental results, we obtained the optimal reaction conditions as follows: CH_3CN (2 mL), catalyst (2 mg), TBHP (2 mmol, 274 μl), styrene (1 mmol, 114 μl), a reaction temperature of 80 °C, and a reaction time of 8 h. The catalytic reactions of compounds **2** and **3** were carried out under the optimum reaction conditions to explore their catalytic activities. As shown in Table 4, the 8 h conversions of compounds **2** and **3** were 94.2% and 92.5%, respectively, and the selectivities for styrene oxides were 58.6% and 76.3%, respectively (Table 4, entries 2 and 3). A comparison of the catalytic data of the three compounds showed that there was little difference in the catalytic oxidation conversion rates of styrene among the three compounds, but the selectivities of the three compounds varied considerably with 58.6% for compound **1**, 58.6% for compound **2** and 76.3% for compound **3**, respectively. This indicates that the vanadium atom-centered polyoxoniobates are more selective for the catalytic oxidation of styrene compared to those centered on Si and P atoms. The presence of a heteroatom has fatal influence to the acidic property of its parent cluster, and a famous example is that $\{PW_{12}O_{40}\}$ is more stable than $\{SiW_{12}O_{40}\}$ under less basic conditions (pH ~ 1.5 *vs.* pH ~ 4.5) and the P heteroatom is more acidic relative to the Si heteroatom.[58] Furthermore, since the V heteroatom is more basic than both Si and P heteroatoms, the V-centered cluster is expected to show more basic properties, resulting in a higher selectivity in the production of styrene oxides.[60]

To explore the catalytic centers, $K_7HNb_6O_{19}$, $CuCl_2$, $CuCl_2$ + enMe, and $VOSO_4$ were also introduced as catalysts into the reaction system (Table 3, entries 4–7). The results showed that the conversion of copper salts was greatly improved, reaching 85.4%, but the contribution to the selectivity of styrene oxide was small, which is only 42.2% (Table 3, entry 5). When a

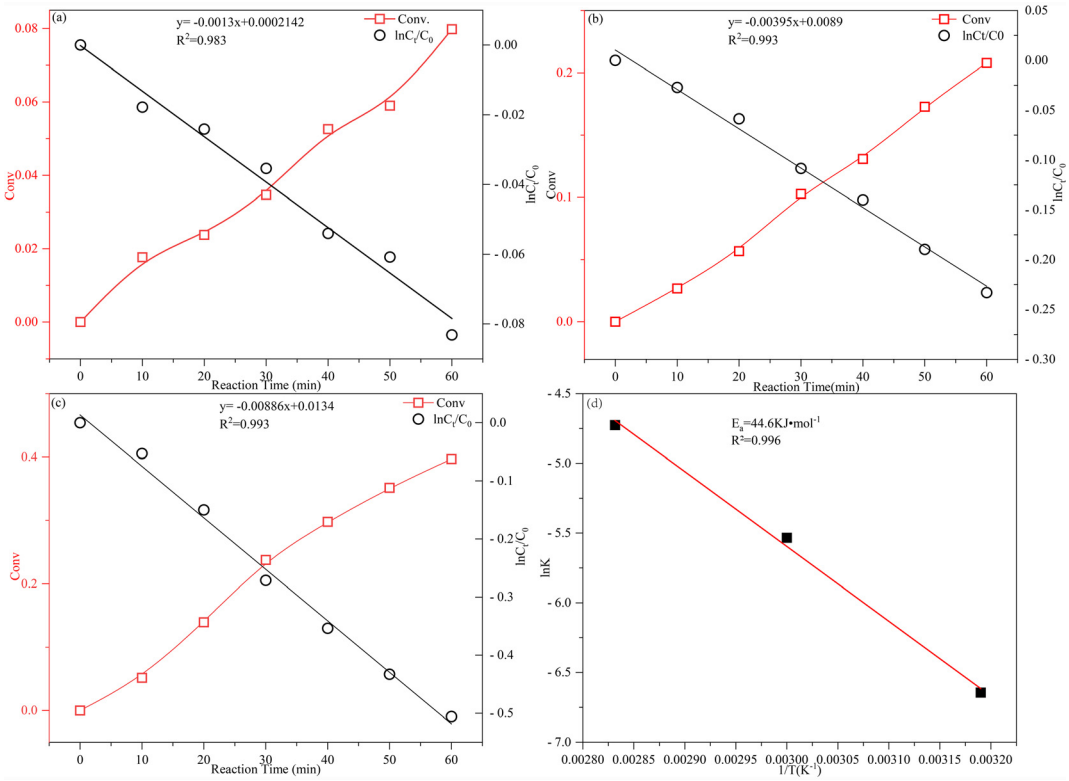

Fig. 4 (a–c) The kinetic profiles of oxidation of styrene catalyzed by compound **1** at 40 °C, 60 °C, and 80 °C; (d) Arrhenius plots of compound **1** according to *k* at different temperatures.

Table 3 Selectivities and conversions of compounds **1–3** and various other contrast catalysts

Entry	Catalysts	Conv. (%)	Product selectivity (mol%)		
			So	Bza	Others
1	Compound **1**	95.2	57.7	36.0	6.3
2	Compound **2**	94.2	58.6	36.2	5.2
3	Compound **3**	92.3	76.3	18.5	5.2
4	$K_7HNb_6O_{19}$ (1.6 mg)	64.5	41.5	55.7	2.8
5	$CuCl_2$ (0.6 mg)	85.4	42.2	46.6	11.2
6	$CuCl_2$ (0.5 mg) + enMe (10 μL)	73.4	61.9	32.9	5.2
7	$VOSO_4$ (0.5 mg)	39.4	6.0	81.7	12.3

Reaction conditions: catalyst (2 mg), for compound **1**: 0.654 μmol, TBHP (2 mM, 274 μL), styrene (1 mM, 114 μL), CH_3CN (2 mL), 80 °C, and 8 h reaction time.

mixture of 1,2-diaminopropane physically combined with the copper salts is used as a catalyst, the conversion decreased to 73.4%. This reduction may be due to the site-blocking effect of the ligand (Table 3, entry 6). Comparing the catalytic results of compounds **1–3** with those of copper salts, as well as the physical mixtures of copper salts and ligands, alongside $K_7HNb_6O_{19}$ and $VOSO_4$ as catalysts, revealed that the main catalytic centers of compounds **1–3** are both the copper atoms and the capped polyoxometalates. These results suggest that compounds **1–3** effectively combine the advantages of clusters and transition metal complexes into a more efficient catalyst, showing a synergistic interaction for high catalytic efficiency. It should be noted that the three compounds are nearly identical to each other; however, the subtle differences of the three compounds in their structures and their stoichiometric compositions will have fatal impact on their catalytic performance. Compound **1** possesses more capping vanadiums compared to compounds **2** and **3**, yet this difference seems to have almost no significant influence on the catalytic performances of the two catalysts. Obviously, both the metal of the metal complexes and the addendum metal of the clusters can act as the catalytic centers of the reaction. Given that the capping vanadium and the addendum niobium atoms belong to the same main group, it is plausible that they exhibit similar catalytic influence on the reaction.[61,62] Thus, we propose that the catalytic similarity between vanadium and niobium is a primary factor underlying the comparable catalytic performances of the three compounds.

In addition, thermal filtration experiments were carried out to study the homogeneity or heterogeneity of the catalyst. Compound **1** was selected and subjected to the filtration experiments. After 4 hours, the solution was filtered through a filtration membrane three times to remove the catalyst, after which the filtrate was allowed to proceed with the reaction for another 4 hours. The data showed that the reaction did not stop even without the catalyst within the catalytic system, which means that compound **1** was partially dissolved in the

solution (Fig. S3†). The ratio $\Delta_{Filt}/\Delta_{Cat}$ serves as a critical parameter for assessing the reaction system, where Δ_{Filt} is the increment in the conversion after the catalyst is filtered out, and Δ_{Cat} is the increment in the unfiltered conversion during the same time interval. $\Delta_{Filt}/\Delta_{Cat} \approx 1$ indicates that the catalyst is a homogeneous catalyst. The $\Delta_{Filt}/\Delta_{Cat}$ of compound **1** was 0.80, indicating that the catalytic activity of compound **1** was predominantly based on the homogeneous system.

Compound **1** did not fully dissolve within the reaction system, and subsequently, we explored the cycling stability of compound **1** and performed cycling performance experiments. After each cycling experiment, the solids present in the system were isolated *via* centrifugation and subsequently washed with acetonitrile. After complete drying at room temperature, the recovered catalyst was utilized in the subsequent catalytic oxidation experiment. As can be seen in Table 4, after four cycles, the reaction conversion slightly decreased from 95.2% to 86.8% and the selectivity for styrene oxide marginally increased. These results indicate that compound **1** exhibited stable catalytic activity over at least 4 cycles. The observed decrease in the conversion may be related to the loss of the catalyst during the cycling process. The infrared (IR) spectra of the catalysts before and after the 4 cycles were compared (Fig. S4†), and it was found that some principal peaks remained unchanged, while some principal peaks disappeared, thereby indicating that a portion of compound **1** had decomposed. The comparison of the XRD spectra of the catalysts was conducted both prior to and following the completion of four cycles. The analysis demonstrates that a portion of compound **1** had lost its crystallinity, confirming the results of its IR spectra.

Moreover, in light of the excellent catalytic efficacy of compound **1** for the oxidation of styrene, we proceeded towards exploring the general applicability of some other olefinic compounds using them as substrates (Table S3†) with toluene as an internal standard for the reactions. Compound **1** showed high catalytic oxidative conversions of cyclohexene and 1-octene of 95.7% and 90.5%, respectively, while demonstrating a moderate conversion of 76.2% for cyclooctene. However, the oxidation of these substrates resulted in lower selectivities towards the peroxide products of the substrate. Such a phenomenon has already been documented in analogous oxidation of alkenes catalyzed by $[ZnWRu_2(Zn_2W_9O_{34})]^{11}$, using *tert*-butyl hydroperoxide as an oxidant.[63]

In order to explore the mechanisms of compounds **1**, **2** and **3** as catalysts to catalyze the oxidation of styrene, we conducted free radical trapping experiments using compound **1** as a representative example. Under the optimal reaction conditions and systems obtained above, molar carbon radical scavengers, such as $CBrCl_3$ and TEMPO (2,2,6,6-tetramethylpiperidine oxide), and the oxygen radical scavenger Ph_2NH (diphenylamine) were added.[64] The experimental results, as shown in Table 5, indicate that all three radical traps have inhibitory effects on the reaction. Specifically, the addition of carbon radical traps ($CBrCl_3$ and TEMPO) had limited inhibition effects on the catalytic oxidation reaction, with inhibition rates of 55.6% and 42.4%, respectively. In contrast, Ph_2NH had the best inhibition effect on the conversion rate of the reaction, achieving a high inhibition rate of 97.7% (Table 5). Collectively, all the above experimental results indicate that the catalytic oxidation of styrene proceeds through the formation of oxygen radical intermediates.

In this context, the most important function of Cu(II) is to decompose the stable hydroperoxide and trigger a radical mechanism.[65] It has been reported that metal ions can decompose TBHP into *tert*-butyl peroxyl radicals *via* a one-electron transfer, where Cu(II) gets reduced to Cu(I) and the electron that is released initiates the radical chain by reacting with TBHP to give *tert*-butyl peroxyl radicals.[66] In the present case, we also believe that the formation of radicals occurs *via* the reduction of Cu(II) to Cu(I). While we propose that the reduction of Cu(II) to Cu(I) in the catalyst leads to the radical initiation process, we must say that the PONbs, synthesized under strongly alkaline conditions and showing very strong basic properties as mentioned above, are very important to suppress the acid-catalyzed epoxide hydrolysis, thus facilitating the formation of styrene oxides.[57] It is widely accepted that hydroperoxo species from polyoxotungstate and polyoxomolybdate are the main catalytic centers for the epoxidation of alkenes using hydrogen peroxide as an oxidant.[67] Polyoxovanadate and polyoxoniobate can also both form similar hydroperoxo species just like those formed from polyoxotungstate and polyoxomolybdate.[61,62] However, in the catalytic system using TBHP as an oxidant, the formation of peroxo radicals from polyoxovanadate and polyoxoniobate in

Table 4 Catalytic effect of cycling experiments on compound **1**

			Product selectivity (mol%)		
Entry	Cycle	Conv. (%)	So	Bza	Others
1	Fresh	95.2	57.7	36.0	6.3
2	1st	94.0	52.7	42.0	5.3
3	2nd	93.6	67.8	27.2	5.0
4	3rd	93.0	60.9	35.5	3.6
5	4th	86.8	62.8	32.0	5.2

Reaction conditions: catalyst (2 mg), for compound **1**: 0.654 μmol, TBHP (2 mM, 274 μL), styrene (1 mM, 114 μL), CH_3CN (2 mL), 80 °C, and 8 h reaction time.

Table 5 Catalysis of compound **1** after the use of radical trapping agents

Entry	Rad. trap	*n* (rad. trap)/*n* (styrene)	Conv. (%)	Conv. drop (%)
1	—	—	95.2	0
2	$CBrCl_3$	1 : 1	42.2	55.7
3	TEMPO	1 : 1	54.8	42.4
4	Ph_2NH	1 : 1	2.19	97.7

Reaction conditions: catalyst (0.0055 mM, 1.0 mg), TBHP (2 mM, 274 μL), styrene (1 mM, 114 μL), acetonitrile (2 mL), radical trap (1 mM), 80 °C, and 8 h reaction time.

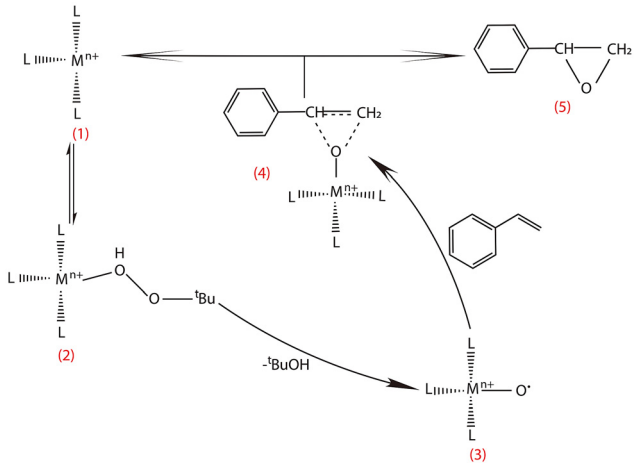

Fig. 5 Mechanism proposed for styrene epoxidation.

conjunction with TBHP cannot be ruled out, as this may occur through a similar homolytic activation mechanism analogous to that of copper atoms to form a radical species.[68] Based on the aforementioned control experiments and free radical trapping studies, we suggest that perhaps both the copper and vanadium atoms as well as niobium atoms are competitive catalytic centers. Based on the exploration of the catalyst active centres in this study, the following one possible mechanism is proposed[69] (Fig. 5). The active metal cation reacts with TBHP to generate a hydroperoxy compound (**2**), species 2 loses a *t*-butanol molecule to render species 3, which reacts with the double-bonded carbon atoms of styrene to form a metalloepoxy intermediate (species 4), and then species 4 decomposes to the intermediate product and regenerates the catalyst. The species 5 can be further oxidized to yield benzaldehyde, phenyl acetaldehyde, benzoic acid and so on (Fig. S5†).

Conclusions

We successfully synthesized three compounds derived from capped polyoxoniobates and copper complexes. Crystal structure analysis found that, despite the three sharing identical cell parameters, compound **1** is not isostructural with compounds **2** and **3**, and compound **1** has different stoichiometric compositions from compounds **2** and **3**. It should be noted that, though the three capped Keggin polyoxoniobates are very similar to each other, they are fundamentally different. The clusters can be divided into two types: bicapped and 4.25-capped clusters. Both the types of clusters can be viewed as intermediates between the traditional Keggin cluster and the fully capped six-capped Keggin cluster. The catalytic properties of the three compounds were investigated as catalysts in the oxidation of styrene with TBHP as the oxidant. Owing to the strongly basic properties of the cluster components of the three catalysts, all the three catalysts demonstrated excellent efficacy in the production of styrene oxide. Notably, for the different nature of the heteroatoms present in the three catalysts, the vanadium-cantered catalyst exhibits the best selectivity towards styrene oxides. The mechanism study found that the catalytic properties of the three catalysts come from the synergistic interactions of the cluster components and the transition metal complex components of the catalysts.

Author contributions

Zhi-Cheng Duan: experiment design, execution of the experiments, data curation, writing – original draft, and writing – review & editing. Guanghua Li and Ke-Chang Li: data collection. Xiao-Bing Cui: experiment design and writing – review & editing.

Data availability

Data are available within the article or its ESI.†.

Conflicts of interest

There are no conflicts to declare.

Acknowledgements

We are thankful for the grant from Jilin Provincial Department of Science and Technology (No. 20190802027ZG).

References

1 D. L. Long, E. Burkholder and L. Cronin, Polyoxometalate clusters, nanostructures and materials: From self assembly to designer materials and devices, *Chem. Soc. Rev.*, 2007, **36**, 105–121.
2 A. Dolbecq, E. Dumas, C. R. Mayer and P. Mialane, Hybrid Organic-Inorganic Polyoxometalate Compounds: From Structural Diversity to Applications, *Chem. Rev.*, 2010, **110**, 6009–6048.
3 X. López, J. J. Carbó, C. Bo and J. M. Poblet, Structure, properties and reactivity of polyoxometalates: a theoretical perspective, *Chem. Soc. Rev.*, 2012, **41**, 7537–7571.
4 Z. M. Zhang, T. Zhang, C. Wang, Z. K. Lin, L. S. Long and W. B. Lin, Photosensitizing metal organic framework enabling visible-light-driven proton reduction by a wells-dawsontype polyoxometalate, *J. Am. Chem. Soc.*, 2015, **137**, 3197–3200.
5 X. B. Han, Z. M. Zhang, T. Zhang, Y. G. Li, W. B. Lin, W. S. You, Z. M. Su and E. B. Wang, Polyoxometalate-based cobalt-phosphate molecular catalysts for visible light-driven water oxidation, *J. Am. Chem. Soc.*, 2014, **136**, 5359–5366.
6 H. J. Lv, Y. V. Geletii, C. C. Zhao, J. W. Vickers, G. B. Zhu, Z. Luo, J. Song, T. Q. Lian, D. G. Musaev and C. L. Hill,

Polyoxometalate water oxidation catalysts and the production of green fuel, *J. Am. Chem. Soc.*, 2012, **41**, 7572–7589.

7 J. W. Zhao, Y. Z. Li, L. J. Chen and G. Y. Yang, Research progress on polyoxometalate-based transition-metal-rare-earth heterometallic derived materials: synthetic strategies, structural overview and functional applications, *Chem. Commun.*, 2016, **52**, 4418–4445.

8 J. Dopta, L. K. Mahnke and W. Bensch, New pronounced progress in the synthesis of group 5 polyoxometalates, *CrystEngComm*, 2020, **22**, 3254–3268.

9 X. X. Li, D. Zhao and S. T. Zheng, Recent advances in POM-organic frameworks and POM-organic polyhedra, *Coord. Chem. Rev.*, 2019, **397**, 220–240.

10 J. Y. Niu, P. T. Ma, H. Y. Niu, J. Li, J. W. Zhao, Y. Song and J. P. Wang, Giant Polyniobate Clusters Based on [Nb7O22] 9- Units Derived from a Nb6O19 Precursor, *Chem. – Eur. J.*, 2007, **13**, 8739–8748.

11 R. P. Bontchev and M. Nyman, Evolution of Polyoxoniobate Cluster Anions, *Angew. Chem., Int. Ed.*, 2006, **45**, 6670–6672.

12 P. Huang, C. Qin, Z. M. Su, Y. Xing, X. L. Wang, K. Z. Shao, Y. Q. Lan and E. B. Wang, Self-Assembly and Photocatalytic Properties of Polyoxoniobates: {Nb24O72}, {Nb32O96}, and {K12Nb96O288} Clusters, *J. Am. Chem. Soc.*, 2012, **134**, 14004–14010.

13 E. J. Graeber and B. Morosin, The molecular configuration of the decaniobate ion ($Nb17O28^{6-}$), *Acta Crystallogr., Sect. B: Struct. Crystallogr. Cryst. Chem.*, 1977, **33**, 2137–2143.

14 R. Tsunashima, D. L. Long, H. N. Miras, D. Gabb, C. P. Pradeep and L. Cronin, The Construction of High-Nuclearity Isopolyoxoniobates with Pentagonal Building Blocks: [HNb27O76]16- and [H10Nb31O93(CO3)]23-, *Angew. Chem., Int. Ed.*, 2010, **49**, 113–116.

15 Y. L. Wu, X. X. Li, Y. J. Qi, H. Yu, L. Jin and S. T. Zheng, {Nb288O768(OH)48(CO3)12}: A Macromolecular Polyoxometalate with Close to 300 Niobium Atoms, *Angew. Chem., Int. Ed.*, 2018, **57**, 8572–8576.

16 P. X. Wu, R. D. Lai, R. Ge, C. Sun, G. Q. Wang, X. X. Li and S. T. Zheng, A Tellurium-Substituted Heteropolyniobate with Unique π–π Stacking and Ionic Conduction Property, *Inorg. Chem.*, 2021, **60**, 6162–6166.

17 Z. Y. Zhang, Q. P. Lin, D. Kurunthu, T. Wu, F. Zuo, S. T. Zheng, C. J. Bardeen, X. H. Bu and P. Y. Feng, Synthesis and Photocatalytic Properties of a New Heteropolyoxoniobate Compound: $K10[Nb2O2(H_2O)2][SiNb12O40]\cdot 12H_2O$, *J. Am. Chem. Soc.*, 2011, **133**, 6934–6937.

18 M. Nyman, F. Bonhomme, T. M. Alam, M. A. Rodriguez, B. R. Cherry, J. L. Krumhans, T. M. Nenoff and A. M. Sattler, A General Synthetic Procedure for Heteropolyniobates, *Science*, 2002, **297**, 996–998.

19 Y. Hou, M. Nyman and M. A. Rodriguez, Soluble Heteropolyniobates from the Bottom of Group IA, *Angew. Chem., Int. Ed.*, 2011, **50**, 12514–12517.

20 N. Li, Y. W. Liu, Y. Lu, D. F. He, S. M. Liu, X. Q. Wang, Y. G. Li and S. X. Liu, An arsenicniobate-based 3D framework with selective adsorption and anion-exchange properties, *New J. Chem.*, 2016, **40**, 2220–2224.

21 Z. J. Liang, J. J. Sun, D. D. Zhang, P. T. Ma, C. Zhang, J. Y. Niu and J. P. Wang, Assembly of TeO32- Ions Embedded in an Nb/O Cage with Selective Decolorization of Organic Dye, *Inorg. Chem.*, 2017, **56**, 10119–10122.

22 J. F. Hu, T. Han, Y. N. Chi, Z. G. Lin, Y. Q. Xu, S. Yang, D. Wei, Y. Z. Zheng and C. W. Hu, Sulfur-centred polyoxoniobate-based 3D organic-inorganic hybrid compound and its magnetic behavior, *Chem. Commun.*, 2016, **52**, 10846–10849.

23 W. W. Guo, H. J. Lv, K. P. Sullivan, W. O. Gordon, A. Balboa, G. W. Wagner, D. G. Musaev, J. Bacsa and C. L. Hill, Broad-Spectrum Liquid- and Gas-Phase Decontamination of Chemical Warfare Agents by One-Dimensional Heteropolyniobates, *Angew. Chem., Int. Ed.*, 2016, **55**, 7403–7407.

24 Z. Y. Zhang, J. Peng, Z. Y. Shi, W. L. Zhou, S. U. Khan and H. S. Liu, Antimony-dependent expansion for the Keggin heteropolyniobate family, *Chem. Commun.*, 2015, **51**, 3091–3093.

25 G. L. Guo, Y. Q. Xu, J. Cao and C. W. Hu, An unprecedented vanadoniobate cluster with 'trans-vanadium' bicapped Keggin-type {VNb12O40(VO)2}, *Chem. Commun.*, 2011, **47**, 9411–9413.

26 J. Q. Shen, Y. Zhang, Z. M. Zhang, Y. G. Li, Y. Q. Gao and E. B. Wang, Polyoxoniobate-based 3D framework materials with photocatalytic hydrogen evolution activity, *Chem. Commun.*, 2014, **50**, 6017–6019.

27 Y. Hou, T. M. Alam, M. A. Rodriguez and M. Nyman, Aqueous compatibility of group IIIA monomers and Nb-polyoxoanions, *Chem. Commun.*, 2012, **48**, 6004–6006.

28 M. Filowitz, R. K. C. Ho, W. G. Klemperer and W. Shum, Oxygen-17 nuclear magnetic resonance spectroscopy of polyoxometalates. 1. Sensitivity and resolution, *Inorg. Chem.*, 1979, **18**, 93–103.

29 G. M. Sheldrick, A short history of SHELX, *Acta Crystallogr., Sect. A: Found. Crystallogr.*, 2008, **64**, 112–122.

30 G. M. Sheldrick, Crystal structure refinement with SHELXL, *Acta Crystallogr., Sect. A: Found. Adv.*, 2015, **71**, 3–8.

31 O. V. Dolomanov, L. J. Bourhis, R. J. Gildea, J. A. K. Howard and H. Puschmann, OLEX2: a complete structure solution, refinement and analysis program, *J. Appl. Crystallogr.*, 2009, **42**, 339–341.

32 H. L. Guo, Y. K. Wang, X. J. Qu, R. Feng, J. Y. Pang, Y. Bai and D. B. Dang, Crystal structure and electrochemistry properties of one two-dimensional heteropolyoxoniobate based on four- and five-vanadium-capped Keggin anions, *New J. Chem.*, 2022, **46**, 1494–1497.

33 I. D. Brown and D. Altermatt, Bond-Valence Parameters Obtained from a Systematic Analysis of the Inorganic Crystal Structure Database, *Acta Crystallogr., Sect. B: Struct. Sci.*, 1985, **41**, 244–247.

34 L. N. Xiao, J. N. Xu, Y. Y. Hu, L. M. Wang, Y. Wang, H. Ding, X. B. Cui and J. Q. Xu, Synthesis and characterizations of the first [V16O39Cl]6-(V16O39) polyanion, *Dalton Trans.*, 2013, **42**, 5247–5251.

35 C. Rocchiccioli-Deltcheff, M. Fournier, R. Franck and R. Thouvenot, Vibrational Investigations of Polyoxometalates. 2. Evidence for Anion-Anion Interactions in Molybdenum(V1) and Tungsten(V1) Compounds Related to the Keggin Structure, *Inorg. Chem.*, 1983, **22**, 207–216.
36 I. V. Kozhevnikov, *Catalysts for Fine Chemical Synthesis, Volume 2, Catalysis by Polyoxometalates*, John Wiley & Sons Ltd, Chichester, UK, 2002.
37 X. J. Song, W. C. Zhu, K. G. Li, J. Wang, H. L. Niu, H. C. Gao, W. X. Zhang, J. H. Yu and M. J. Jia, Epoxidation of olefins with oxygen/isobutyraldehyde over transition-metal-substituted phosphomolybdic acid on SBA-15, *Catal. Today*, 2016, **259**, 59–65.
38 T. Okuhara, N. Mizuno and M. Misono, Catalytic Chemistry of Heteropoly Compounds, *Adv. Catal.*, 1996, **41**, 113–252.
39 P. Cancino, V. Paredes-García, P. Aguirre and E. Spodine, A reusable CuII based metal-organic framework as a catalyst for the oxidation of olefins, *Catal. Sci. Technol.*, 2014, **4**, 2599–2607.
40 J. L. Hu, K. X. Li, W. Li, F. Y. Ma and Y. H. Guo, Selective oxidation of styrene to benzaldehyde catalyzed by Schiff base-modified ordered mesoporous silica materials impregnated with the transition metal-monosubstituted Keggin-type polyoxometalates, *Appl. Catal., A*, 2009, **364**, 211–220.
41 C. M. Granadeiro, A. D. S. Barbosa, P. Silva, F. A. A. Paz, V. K. Saini, J. Pires, B. D. Castro, S. S. Balula and L. Cunha-Silva, Monovacant polyoxometalates incorporated into MIL-101(Cr): novel heterogeneous catalysts for liquid phase oxidation, *Appl. Catal., A*, 2013, **453**, 316–326.
42 R. Sadasivan, A. Patel and A. Ballabh, Investigation of catalytic properties of Cs salt of di-copper substituted phosphotungstate, Cs7[PW10Cu2(H_2O)O38] in epoxidation of styrene, *Inorg. Chim. Acta*, 2019, **487**, 345–353.
43 R. Sadasivan and A. Patel, Mono-copper substituted phosphotungstate supported on to neutral alumina: Synthesis, characterization and detailed studies for oxidation of styrene, *Inorg. Chim. Acta*, 2021, **522**, 120357.
44 C. M. Granadeiro, P. Silva, V. K. Saini, F. A. A. Paz, J. Pires, L. Cunha-Silva and S. S. Balula, Novel heterogeneous catalysts based on lanthanopolyoxometalates supported on MIL-101(Cr), *Catal. Today*, 2013, **218–219**, 35–42.
45 S. S. Balula, C. M. Granadeiro, A. D. S. Barbosa, I. C. M. S. Santos and L. Cunha-Silva, Multifunctional catalyst based on sandwich-type polyoxotungstate and MIL-101 for liquid phase oxidations, *Catal. Today*, 2013, **210**, 142–148.
46 P. A. Shringarpure and A. Patel, Supported undecatungstophosphate: An efficient recyclable bi-functional catalyst for esterification of alcohols as well as selective oxidation of styrene, *Chem. Eng. J.*, 2011, **173**, 612–619.
47 P. A. Shringarpure and A. Patel, Liquid phase oxidation of styrene over zirconia supported undecatungstophosphate using different oxidants: a comparative study, *Dalton Trans.*, 2010, **39**, 2615–2621.
48 E. Poli, R. D. Sousa, F. Jérome, Y. Pouilloux and J. Clacens, Catalytic epoxidation of styrene and methyl oleate over peroxophosphotungstate entrapped in mesoporous SBA-15, *Catal. Sci. Technol.*, 2012, **2**, 910–914.
49 N. Narkhede, A. Patel and S. Singh, Mono lacunary phosphomolybdate supported on MCM-41: synthesis, characterization and solvent free aerobic oxidation of alkenes and alcohols, *Dalton Trans.*, 2014, **43**, 2512–2520.
50 L. S. Nogueira, S. Ribeiro, C. M. Granadeiro, E. Pereira, G. Feio, L. Cunha-Silva and S. S. Balula, Novel polyoxometalate silica nano-sized spheres: efficient catalysts for olefin oxidation and the deep desulfurization process, *Dalton Trans.*, 2014, **43**, 9518–9528.
51 P. Sharma and A. Patel, Supported 12-molybdophosphoricacid: Characterization and non-solvent liquid phase oxidation of styrene, *J. Mol. Catal. A: Chem.*, 2009, **299**, 37–43.
52 J. Tang, X. L. Yang, X. W. Zhang, M. Wang and C. D. Wu, A functionalized polyoxometalate solid for selective oxidation of styrene to benzaldehyde, *Dalton Trans.*, 2010, **39**, 3396–3399.
53 T. A. G. Duarte, I. C. M. S. Santos, M. M. Q. Simões, M. G. P. M. S. Neves, A. M. V. Cavaleiro and J. A. S. Cavaleiro, Homogeneous Catalytic Oxidation of Olefins with Hydrogen Peroxide in the Presence of a Manganese-Substituted Polyoxomolybdate, *Catal. Lett.*, 2013, **144**, 104–111.
54 S. S. Balula, L. Cunha-Silva, I. C. M. S. Santos, A. C. Estrada, A. C. Fernandes, J. A. S. Cavaleiro, J. Pires, C. Freire and A. M. V. Cavaleiro, Mono-substituted silicotungstates as active catalysts for sustainable oxidations: homo- and heterogeneous performance, *New J. Chem.*, 2013, **37**, 2341–2350.
55 T. A. G. Duarte, A. E. Estrada, M. M. Q. Simões, I. C. M. S. Santos, A. M. V. Cavaleiro, M. G. P. M. S. Neves and J. A. S. Cavaleiro, Homogeneous catalytic oxidation of styrene and styrene derivatives with hydrogen peroxide in the presence of transition metal-substituted polyoxotungstates, *Catal. Sci. Technol.*, 2015, **5**, 351–363.
56 R. Sadasivan and A. Patel, Flexible oxidation of styrene using TBHP over zirconia supported mono-copper substituted phosphotungstate, *RSC Adv.*, 2019, **48**, 27755–27767.
57 P. Liu, H. Wang, Z. C. Feng, P. L. Ying and C. Li, Direct immobilization of self-assembled polyoxometalate catalyst in layered double hydroxide for heterogeneous epoxidation of olefins, *J. Catal.*, 2008, **256**, 345–348.
58 M. T. Pope, *Heteropoly and Isopoly Oxometalate*, Springer-Verlag, Berlin, Heidelberg, New York, Tokyo, 1983.
59 X. D. Yu, L. L. Xu, X. Yang, Y. N. Guo, K. X. Li, J. L. Hu, W. Li, F. Y. Ma and Y. H. Guo, Preparation of periodic mesoporous silica-included divacant Keggin units for the catalytic oxidation of styrene to synthesize styrene oxide, *Appl. Surf. Sci.*, 2008, **254**, 4444–4451.
60 N. V. Maksimchuk, K. A. Kovalenko, S. S. Arzumanov, Y. A. Chesalov, M. S. Melgunov, A. G. Stepanov, V. P. Fedin and O. A. Kholdeeva, Hybrid Polyoxotungstate/MIL-101 Materials: Synthesis, Characterization, and Catalysis of

H_2O_2-Based Alkene Epoxidation, *Inorg. Chem.*, 2010, **49**, 2920–2930.

61 C. A. Ohlin, E. M. Villa, J. C. Fettinger and W. H. Casey, Distinctly Different Reactivities of Two Similar Polyoxoniobates with Hydrogen Peroxide, *Angew. Chem., Int. Ed.*, 2008, **47**, 8251–8254.

62 M. Bühl, R. Schurhammer and P. Imhof, Peroxovanadate Imidazole Complexes as Catalysts for Olefin Epoxidation: Density Functional Study of Dynamics, 51 V NMR Chemical Shifts, and Mechanism, *J. Am. Chem. Soc.*, 2004, **126**, 3310–3320.

63 R. Neumann and A. M. Khenkin, Noble Metal (RuIII, PdII, PtII) Substituted "Sandwich" Type Polyoxometalates: Preparation, Characterization, and Catalytic Activity in Oxidations of Alkanes and Alkenes by Peroxides, *Inorg. Chem.*, 1995, **34**, 5753–5760.

64 A. M. Kirillov, M. N. Kopylovich, M. V. Kirillova, E. Y. Karabach, M. Haukka, M. F. C. G. D. Silva and A. J. L. Pombeiro, Mild Peroxidative Oxidation of Cyclohexane Catalyzed by Mono-, Di-, Tri-, Tetra- and Polynuclear Copper Triethanolamine Complexes, *Adv. Synth. Catal.*, 2006, **348**, 159–174.

65 M. M. Hossain, W. K. Huang, H. J. Chen, P. H. Wang and S. G. Shyu, Efficient and selective copper-catalyzed organic solvent-free and biphasic oxidation of aromatic gem-disubstituted alkenes to carbonyl compounds by tert-butyl hydroperoxide at room temperature, *Green Chem.*, 2014, **16**, 3013–3017.

66 M. Salavati-Niasari, M. Shaterian, M. R. Ganjali and P. Norouzi, Oxidation of cyclohexene with tert-butylhydroperoxide catalysted by host (nanocavity of zeolite-Y)/guest (Mn(II), Co(II), Ni(II) and Cu(II) complexes of N,N'-bis(salicylidene)phenylene-1,3-diamine) nanocomposite materials (HGNM), *J. Mol. Catal. A: Chem.*, 2007, **261**, 147–155.

67 K. Kamata, M. Kotani, K. Yamaguchi, S. Hikichi and N. Mizuno, Olefin Epoxidation with Hydrogen Peroxide Catalyzed by Lacunary Polyoxometalate [γ-SiW10O34(H_2O)2]4-, *Chem. – Eur. J.*, 2006, **13**, 639–648.

68 D. W. Hu, X. J. Song, S. J. Wu, X. T. Yang, H. Zhang, X. Y. Chang and M. J. Jia, Solvothermal synthesis of Co-substituted phosphomolybdate acid encapsulated in the UiO-66 framework for catalytic application in olefin epoxidation, *Chin. J. Catal.*, 2021, **42**, 356–366.

69 Y. L. Liang, C. Y. Yi, S. Tricard, J. Fang, J. H. Zhao and W. G. Shen, Prussian blue analogues as heterogeneous catalysts for epoxidation of styrene, *RSC Adv.*, 2015, **5**, 17993–17999.